

FUSING IN 3D: FREE-VIEWPOINT FUSION RENDERING WITH A 3D INFRARED-VISIBLE SCENE REPRESENTATION

Chao Yang, Deshui Miao*, Chao Tian, Guoqing Zhu, Yameng Gu and Zhenyu He***

School of Computer Science and Technology, Harbin Institute of Technology, Shenzhen

ABSTRACT

Infrared-visible image fusion aims to integrate infrared and visible information into a single fused image. Existing 2D fusion methods focus on fusing images from fixed camera viewpoints, neglecting a comprehensive understanding of complex scenarios, which results in the loss of critical information about the scene. To address this limitation, we propose a novel Infrared-Visible Gaussian Fusion (IVGF) framework, which reconstructs scene geometry from multimodal 2D inputs and enables direct rendering of fused images. Specifically, we propose a cross-modal adjustment (CMA) module that modulates the opacity of Gaussians to solve the problem of cross-modal conflicts. Moreover, to preserve the distinctive features from both modalities, we introduce a fusion loss that guides the optimization of CMA, thus ensuring that the fused image retains the critical characteristics of each modality. Comprehensive qualitative and quantitative experiments demonstrate the effectiveness of the proposed method.

Index Terms— 3D Gaussian Splatting, Infrared-Visible Fusion, Multi-modal Representation

1. INTRODUCTION

Infrared-visible image fusion merges thermal radiation information from infrared images with textural details from visible images to produce a comprehensive fused representation, leveraging their complementary characteristics under varying illumination conditions. The fused results significantly benefit various computer vision tasks, including object detection [1, 2], tracking [3, 4], and semantic segmentation [5, 6]. However, traditional 2D image fusion methods are limited to pixel-level integration from fixed camera perspectives, which constrains their applicability in scene understanding tasks.

Nowadays, multimodal scene representation introduces a novel paradigm that enables free-viewpoint rendering through multi-view 2D inputs, providing a more comprehensive representation of scene information. ThermalGaussian [7] introduced a 3DGS-based [8] scene representation for infrared and visible modalities. MMOne [9] proposed a Gaussian-based multimodal decoupled representation that splits Gaussians into modality-specific and shared features to capture distinct modal characteristics separately. MS-Splatting [10] introduced a multi-spectral view synthesis framework that replaces traditional spherical harmonics with a unified neural color representation. However, current multimodal scene representation methods are limited to separate-modality rendering and lack the capability for rendering fused images. As shown in Figure 1(c), modality conflicts in multimodal 3DGS often cause cross-modal error accumulation during direct rendering, resulting in the loss of critical

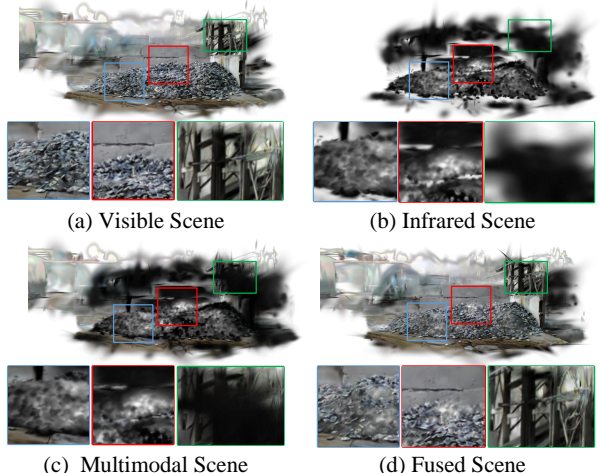


Fig. 1. 3D Gaussian scene representation. (a) Visible 3D scene. (b) Infrared 3D scene. (c) Multimodal 3D scene. (d) Our Infrared-Visible Gaussian Fusion (IVGF) scene. Direct rendering from multimodal scenes introduces cumulative errors, leading to the loss of detail and infrared information.

information from both modalities. An alternative approach employs a render-then-fusion pipeline that first renders each modality separately before fusing them, but this method incurs high computational overhead.

To overcome these limitations, we propose Infrared-Visible Gaussian Fusion (IVGF), a novel 3D multimodal fusion framework that enables direct rendering of fused images from arbitrary viewpoints. Specifically, to resolve modality conflicts during rendering, we introduce a cross-modal adjustment (CMA) module that modulates the opacity parameters of multimodal Gaussians based on their color attributes. Furthermore, to ensure the fused images retain salient characteristics from both modalities, we design a specialized fusion loss that preserves modality-specific features, thereby enhancing the overall rendering quality. As demonstrated in Figure 1(d) (blue/red/green boxes), IVGF effectively preserves both infrared radiation characteristics and visible structural details, enabling comprehensive and informative scene characterization.

Our key contributions are summarized as follows:

- We propose Infrared-Visible Gaussian Fusion (IVGF), the first multimodal fusion representation framework that enables free-viewpoint rendering of fused images.
- We introduce cross-modal adjustment (CMA) module that adjusts Gaussian opacity parameters to resolve modality conflicts during multimodal rendering.
- We propose a fusion loss that preserves critical modality-

* Equal contribution

** Corresponding Author

Email: {20b951014, 22b951002, tianchao, 20b951002, 23b951001}@stu.hit.edu.cn, zhenyuhe@hit.edu.cn.

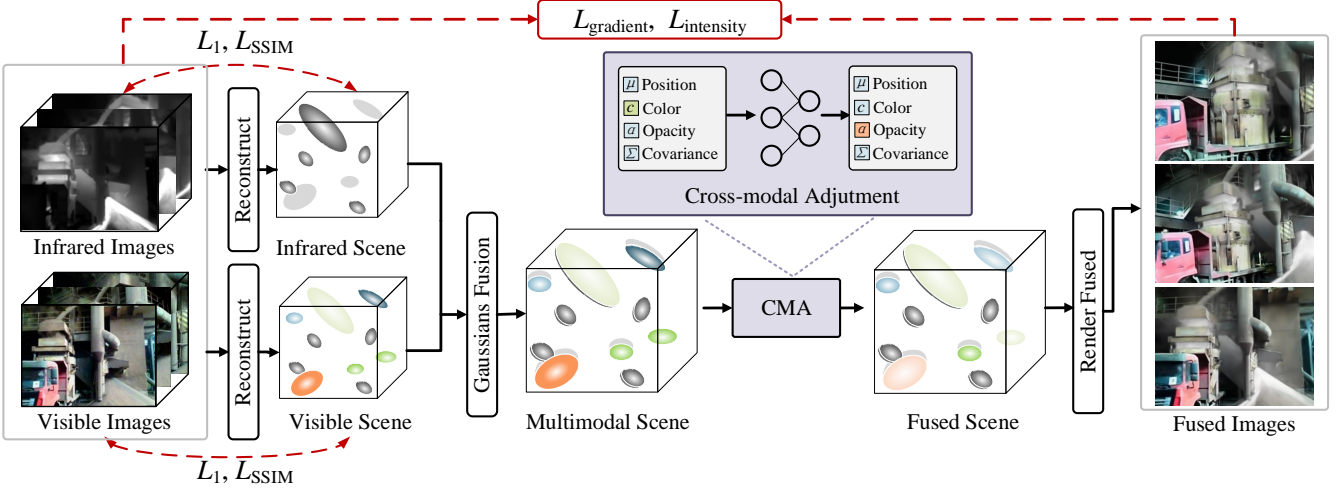


Fig. 2. Overview of our Infrared-Visible Gaussian Fusion (IVGF) framework. First, infrared and visible Gaussians are trained separately. Subsequently, they are concatenated and processed by a cross-modal adjustment (CMA) module, which refines the parameters of Gaussians to reconstruct a fused 3D scene.

specific features, which can obtain high rendering fidelity.

2. METHODOLOGY

Traditional 2D image fusion methods are constrained by fixed camera viewpoints, thereby limiting their applicability in downstream tasks. To overcome this limitation, we propose a novel framework that reconstructs a fused infrared-visible 3D scene representation, enabling the rendering of fused images from arbitrary viewpoints.

2.1. Preliminaries: 3D Gaussian Splatting

3D Gaussian Splatting (3DGS) framework [8], which provides an efficient differentiable representation for radiance fields. The scene is represented as a collection $\mathcal{G} = \{g_i\}_{i=1}^N$ of anisotropic 3D Gaussians, where each Gaussian primitive g_i represents a point in the scene and is parameterized by several essential attributes. The mean position $\mu_i \in \mathbb{R}^3$ defines the spatial location of each Gaussian in 3D space, while the covariance matrix $\Sigma_i = \mathbf{R}_i \mathbf{S}_i \mathbf{S}_i^\top \mathbf{R}_i^\top \in \mathbb{R}^{3 \times 3}$ controls its anisotropic scaling through the scaling matrix \mathbf{S}_i and its orientation via the rotation matrix \mathbf{R}_i . Each Gaussian also possesses an opacity value $\alpha_i \in [0, 1]$ that determines its contribution to the final rendered image, along with view-dependent color properties \mathbf{c}_i encoded through spherical harmonics coefficients.

2.2. Infrared-Visible Gaussian Representation

Due to the modality conflicts, direct rendering of fused images using multimodal 3DGS remains challenging. As demonstrated in Figure 3 (c), rendered results often suffer from significant information loss, in which key structural details are obscured and critical infrared signatures are inadequately preserved. To address this challenge, we propose a novel framework for 3DGS-based fused scene representation as shown in Figure 2. The pipeline first constructs dual-modal scene representations, then optimizes the cross-modal adjustment (CMA) module to adjust opacity parameter to resolve modality conflicts during rendering. The multimodal fusion rendering $F(\mathbf{x})$ at coordinate $\mathbf{x} \in \mathbb{R}^2$ is computed as follows:

$$F(\mathbf{x}) = \sum_{k=1}^{N+M} c_k (\tau_k \alpha_k) \prod_{j=1}^{k-1} (1 - \tau_j \alpha_j), \quad (1)$$

where N and M denotes visible and infrared Gaussians contribute to the pixel, c_k represents the color of the k -th Gaussian, α_k is its opacity, and τ_k denotes the cross-modal attention weight predicted by the cross-modal adjustment (CMA) module.

CMA adjusts the opacities of infrared and visible Gaussians through a learned modality-aware MLP mechanism. Specifically, the spherical harmonics coefficients c_{inf} and c_{vis} of the two Gaussians are concatenated and fed to MLP to predict τ :

$$\tau = \text{MLP}(\text{Concat}(c_{\text{inf}}, c_{\text{vis}})), \quad (2)$$

where $\tau \in [0, 1]$ dynamically scales the opacity parameter of each Gaussian and $c \in \mathbb{R}^{(N+M) \times d_c}$, with d_c denoting the dimension of the spherical harmonics coefficients per Gaussian. The MLP is calculated as follows:

$$\text{MLP}(\mathbf{C}) = \sigma \left(\mathbf{W}_3^\top \cdot \phi_2(\phi_1(\mathbf{C})) \right), \quad (3)$$

$$\phi_i(\mathbf{x}) = \text{LayerNorm}(\text{LeakyReLU}(\mathbf{x} \mathbf{W}_i + \mathbf{b}_i)) \quad (i = 1, 2), \quad (4)$$

where \mathbf{W} are weight matrices, σ is the output activation function, and ϕ includes LeakyReLU activation and layer normalization.

2.3. Loss Function

We adapt a two-stage training strategy for Infrared-Visible Gaussian Fusion (IVGF). In the first stage, 3D representation of the two modalities are trained using the same set up of ThermalGaussian [7]. In the second stage, two Gaussians are concatenated, and the cross-modal adjustment (CMA) module is trained to obtain the fused Gaussian representation.

Training Stage 1. Following ThermalGaussian [7], the Gaussian representations of the two modalities are trained separately. The loss function is formulated as:

$$\mathcal{L}_{\text{stage 1}} = \gamma \mathcal{L}_{\text{Visible}} + (1 - \gamma) \mathcal{L}_{\text{Infrared}}, \quad (5)$$

$$\mathcal{L}_{\text{Visible}} = \|V - V_{\text{render}}\|_1 + (1 - \text{SSIM}(V, V_{\text{render}})), \quad (6)$$

$$\mathcal{L}_{\text{Infrared}} = \|T - T_{\text{render}}\|_1 + (1 - \text{SSIM}(T, T_{\text{render}})). \quad (7)$$

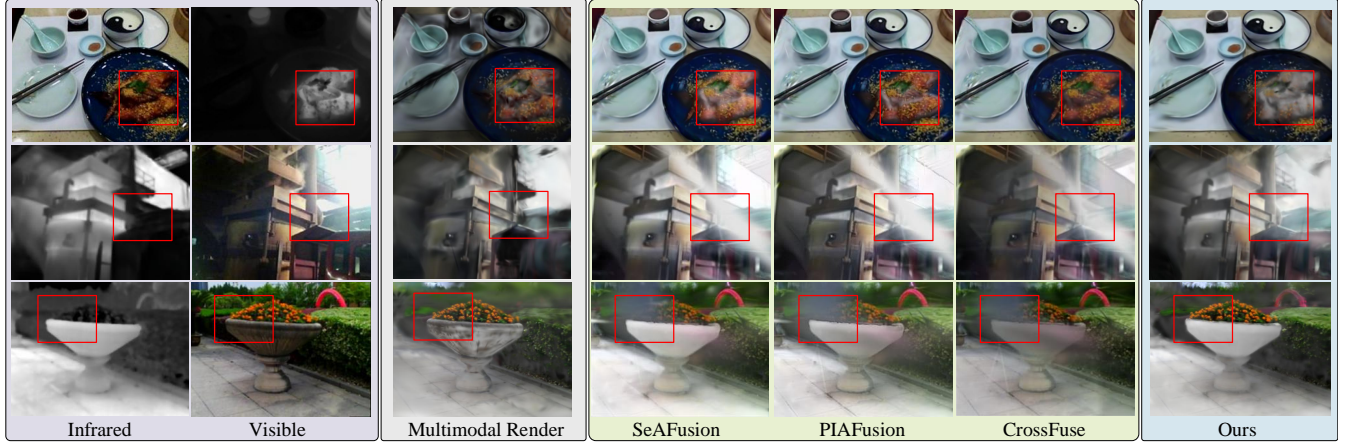


Fig. 3. Qualitative results of different methods. The first box contains infrared and visible images, the second box shows the results of multimodal rendering, the third box presents the fusion results from the render-then-fusion methods, and the final box displays our results.

Here V denotes visible image, T denotes thermal infrared image, and $\|\cdot\|_1$ denotes the ℓ_1 distance, $\text{SSIM}(\cdot, \cdot)$ denotes the structural similarity index, and the coefficient $\gamma = N_{\text{Infrared}} / (N_{\text{Infrared}} + N_{\text{Visible}})$ balances the contributions of the visible and infrared modalities, where N_{Infrared} and N_{Visible} denote the numbers of Gaussians in the corresponding modalities.

Training Stage 2. To optimize a multimodal fused scene that preserves salient information from both modalities, we propose a novel fusion loss function to guide the cross-modal adjustment (CMA) module learning. Let I_{fuse} denote the fused image rendered by the 3D fusion scene. The stage 2 cross-modal fusion loss function is formulated as:

$$\mathcal{L}_{\text{stage 2}} = \mathcal{L}_{\text{intensity}} + \mathcal{L}_{\text{gradient}}, \quad (8)$$

where $\mathcal{L}_{\text{intensity}}$ combines pixel-level similarity and structural similarity measures.

$$\begin{aligned} \mathcal{L}_{\text{intensity}} = & \lambda_1 \|I_{\text{fuse}} - \max(V, T)\|_1 \\ & + \lambda_2 (1 - \text{SSIM}(I_{\text{fuse}}, T) + (1 - \text{SSIM}(I_{\text{fuse}}, V))), \end{aligned} \quad (9)$$

and $\mathcal{L}_{\text{gradient}}$ promotes edge retention between the two modalities, which is defined as follows:

$$\mathcal{L}_{\text{gradient}} = \|\nabla I_{\text{fuse}} - \nabla \max(V, T)\|_1, \quad (10)$$

where ∇ denotes the spatial gradient operator. The weighting parameters λ_1 and λ_2 balance between intensity preservation and structural maintenance. The proposed loss function helps preserve the most important information, thereby enhancing the representation capability of the fused multimodal scene.

3. EXPERIMENTS

3.1. Experimental Setup

Datasets. RGBT-Scenes dataset [7] contains over 1,000 aligned visible and thermal infrared image pairs. The dataset covers 10 diverse categories of scenes, including indoor and outdoor environments.

Evaluation Metrics. Following the evaluation methodology for 2D fusion performance, we first calculate metrics between the fused image and the two source images, then average the metrics to assess overall performance. The metrics used for evaluation include: Peak

Signal-to-Noise Ratio (PSNR), Structural Similarity Index (SSIM), and Learned Perceptual Image Patch Similarity (LPIPS).

Implement Details. Our IVGF framework is built upon Thermal-Gaussian [7], adopting all experimental parameters from the base model. The training process consisted of 30k iterations (15k for separate reconstruction phase followed by 15k for CMA optimization) on an RTX 3090 Ti GPU, generating fused images at a resolution of 640×480 . For the loss function in Equation 9, we set the weights to $\lambda_1 = 1$ and $\lambda_2 = 2$.

Compared methods. We adapt a render-then-fusion pipeline to generate fused images for evaluation and comparison. Specifically, ThermalGaussian [7] first renders paired infrared and visible images, and the two rendered images are then fed into state-of-the-art fusion methods to obtain the fused results, including CDDFuse [11], CrossFuse [12], EMMA [13], LRRNet [14], LiMFusion [15], PIAFusion [16], SHIP [17], SeAFusion [18], and SwinFusion [19].

3.2. Qualitative Analysis of Fusion Methods

Figure 3 compares the results of our method with direct multimodal 3DGS rendering results and other 2D fusion methods. Rendering of multimodal 3DGS result leads to an accumulation of errors, resulting in blurry images and the loss of critical information. For 2D fusion methods (render-then-fusion strategy), the regions within the red bounding boxes tend to lose critical thermal information and exhibit blurring as well as abrupt illumination changes. In contrast, our method effectively preserves the thermal information from the infrared modality and the textural details from the visible modality, avoiding these artifacts. These comparisons demonstrate that our proposed IVGF effectively preserves and integrates information from both modalities, achieving a more comprehensive multimodal fusion representation.

3.3. Quantitative Analysis of Fusion Methods

The quantitative comparisons in Table 1 show that IVGF achieves the highest scores in SSIM and LPIPS across almost all scenes, outperforming nine existing fusion methods (red denotes the best performance, blue the second-best). The results demonstrate that our proposed IVGF can effectively reconstruct fused multimodal scenes and produce higher-quality fusion results than 2D fusion methods (render-then-fusion strategy).

Table 1. Quantitative performance comparison with 2D fusion methods (best in Red, second best in Blue). The \uparrow arrow indicates that higher values are better, while the \downarrow arrow indicates that lower values are better.

Method	Daily Stuff	Dimsum	Glass Cup	Iron Ingot	Land Scape	Parterre	Plant Equipment	Road Block	Rotary Kiln	Truck
LPIPS \downarrow	CDDFuse (CVPR 2023)	0.462	0.392	0.384	0.420	0.505	0.429	0.380	0.399	0.359
	CrossFuse (IF 2024)	0.452	0.391	0.409	0.408	0.495	0.408	0.368	0.373	0.362
	EMMA (CVPR 2024)	0.475	0.406	0.414	0.428	0.535	0.440	0.389	0.412	0.405
	LRRNet (TPAMI 2023)	0.448	0.380	0.375	0.422	0.512	0.417	0.368	0.391	0.360
	LiMFusion (OLEN 2024)	0.494	0.428	0.456	0.427	0.528	0.441	0.396	0.424	0.401
	PIAFusion (IF 2022)	0.453	0.393	0.381	0.416	0.515	0.426	0.387	0.378	0.391
	SHIP (CVPR 2024)	0.525	0.445	0.398	0.463	0.604	0.522	0.483	0.460	0.517
	SeAFusion (IF 2022)	0.452	0.389	0.380	0.415	0.521	0.423	0.378	0.384	0.381
PSNR \uparrow	SwinFusion (JAS 2022)	0.459	0.385	0.376	0.418	0.517	0.428	0.377	0.396	0.367
	Ours	0.425	0.378	0.371	0.413	0.481	0.395	0.370	0.366	0.369
	CDDFuse (CVPR 2023)	13.275	12.495	12.861	13.786	13.966	15.112	14.059	15.105	13.755
	CrossFuse (IF 2024)	14.260	14.018	12.711	15.134	15.056	16.531	15.549	15.945	15.168
	EMMA (CVPR 2024)	13.519	12.438	12.718	14.042	14.395	14.832	14.506	14.972	13.916
	LRRNet (TPAMI 2023)	14.469	13.590	14.197	14.597	14.630	15.814	15.624	14.765	14.839
	LiMFusion (OLEN 2024)	12.997	12.536	12.877	14.050	14.055	15.432	14.303	14.547	12.895
	PIAFusion (IF 2022)	13.947	13.507	13.918	14.771	13.756	15.659	14.407	15.084	12.027
SSIM \uparrow	SHIP (CVPR 2024)	9.073	9.608	12.569	10.412	6.116	9.397	8.878	9.072	5.859
	SeAFusion (IF 2022)	13.127	12.812	13.473	13.878	13.706	14.677	13.826	14.049	12.852
	SwinFusion (JAS 2022)	12.976	12.573	13.205	13.944	13.702	14.320	13.701	14.857	12.368
	Ours	13.929	14.738	12.968	14.553	15.579	16.646	15.047	15.620	12.592
	CDDFuse (CVPR 2023)	0.614	0.541	0.577	0.490	0.572	0.696	0.657	0.808	0.575
	CrossFuse (IF 2024)	0.613	0.544	0.570	0.490	0.558	0.707	0.661	0.831	0.552
	EMMA (CVPR 2024)	0.602	0.545	0.575	0.489	0.548	0.685	0.652	0.805	0.559
	LRRNet (TPAMI 2023)	0.630	0.540	0.592	0.484	0.552	0.682	0.648	0.802	0.553
SSIM \uparrow	LiMFusion (OLEN 2024)	0.601	0.535	0.570	0.484	0.540	0.681	0.648	0.792	0.561
	PIAFusion (IF 2022)	0.615	0.548	0.593	0.489	0.531	0.695	0.647	0.812	0.557
	SHIP (CVPR 2024)	0.526	0.484	0.568	0.442	0.428	0.591	0.531	0.729	0.413
	SeAFusion (IF 2022)	0.619	0.555	0.596	0.495	0.559	0.703	0.662	0.812	0.582
	SwinFusion (JAS 2022)	0.616	0.553	0.591	0.494	0.559	0.692	0.661	0.807	0.586
	Ours	0.665	0.567	0.613	0.495	0.610	0.734	0.680	0.839	0.618
										0.603



Fig. 4. Ablation study on the effects of different modules. The cross-modal adjustment (CMA) module resolves cross-modal error accumulations, while the proposed fusion loss ensures the retention of essential features from both modalities in the rendered results.

3.4. Ablation Study

Comparison with different 3D fusion strategies. As shown in Figure 3 and Table 2.1, our method achieves a more favorable balance among visual quality, storage efficiency, and rendering speed. Specifically, IVGF outperforms multimodal rendering in all performance metrics while matching its memory and speed. Compared to the 2D render-then-fusion strategy, IVGF achieves superior performance with higher PSNR and SSIM, lower LPIPS, a faster speed of 182 FPS, and a reduced memory usage of 48 MB. These results demonstrate that IVGF establishes an effective and efficient new paradigm for 3D scene representation.

Effect of different modules. As shown in Figure 4 and Table 2.2, ablation study shows that the cross-modal adjustment (CMA) module enhances structural details, leading to improvements in visual

Table 2. Ablation study of our method. (Best in Red, Second Best in Blue). The \uparrow arrow indicates that higher values are better, while the \downarrow arrow indicates that lower values are better.

Methods	LPIPS \downarrow	PSNR \uparrow	SSIM \uparrow	Mem. \downarrow	FPS \uparrow
1	Multimodal Render	0.408	12.426	0.515	20 MB
	2D Fusion	0.389	12.812	0.555	69 MB
2	One-stage training	0.503	10.735	0.455	376 MB
	+ CMA	0.371	14.660	0.567	23 MB
	+ CMA + L_{stage2}	0.378	14.738	0.567	21 MB

quality, evaluation metrics, processing speed, and memory efficiency. This improvement stems from the CMA module's ability to effectively resolve conflicts between multimodal Gaussians, thereby achieving higher performance than one-stage training strategy. Moreover, with the proposed fusion loss, visual results exhibit enhanced retention of salient information from both modalities, while quantitative evaluations confirm consistent improvements across all metrics. This demonstrates that our proposed loss function effectively preserves critical features from each modality within the fused multimodal scene representation.

4. CONCLUSION

In this work, we present Infrared-Visible Gaussian Fusion (IVGF), the first framework to achieve free-viewpoint rendering of fused images through a multimodal fusion 3D representation. To this end, we design a cross-modal adjustment (CMA) module to resolve modality conflicts by dynamically modulating Gaussian opacity and introduce a novel fusion loss to retain salient information from two modalities. Extensive experiments validate the effectiveness of our approach.

5. REFERENCES

- [1] Hongxu Yin, Arash Vahdat, Jose M Alvarez, Arun Mallya, Jan Kautz, and Pavlo Molchanov, “A-vit: Adaptive tokens for efficient vision transformer,” in *Proceedings of the IEEE/CVF conference on computer vision and pattern recognition*, 2022, pp. 10809–10818.
- [2] Chao Tian, Zikun Zhou, Yuqing Huang, Gaojun Li, and Zhenyu He, “Cross-modality proposal-guided feature mining for unregistered rgb-thermal pedestrian detection,” *IEEE Transactions on Multimedia*, vol. 26, pp. 6449–6461, 2024.
- [3] Seokju Cho, Jiahui Huang, Seungryong Kim, and Joon-Young Lee, “Flowtrack: Revisiting optical flow for long-range dense tracking,” in *Proceedings of the IEEE/CVF Conference on Computer Vision and Pattern Recognition*, 2024, pp. 19268–19277.
- [4] Xiao Wang, Xiujun Shu, Shiliang Zhang, Bo Jiang, Yaowei Wang, Yonghong Tian, and Feng Wu, “Mfgnet: Dynamic modality-aware filter generation for rgb-t tracking,” *IEEE Transactions on Multimedia*, vol. 25, pp. 4335–4348, 2022.
- [5] Alexander Kirillov, Eric Mintun, Nikhila Ravi, Hanzi Mao, Chloe Rolland, Laura Gustafson, Tete Xiao, Spencer Whitehead, Alexander C Berg, Wan-Yen Lo, et al., “Segment anything,” in *Proceedings of the IEEE/CVF international conference on computer vision*, 2023, pp. 4015–4026.
- [6] Ying Lv, Zhi Liu, and Gongyang Li, “Context-aware interaction network for rgb-t semantic segmentation,” *IEEE Transactions on Multimedia*, vol. 26, pp. 6348–6360, 2024.
- [7] Rongfeng Lu, Hangyu Chen, Zunjie Zhu, Yuhang Qin, Ming Lu, Le Zhang, Chenggang Yan, and Anke Xue, “Thermal-gaussian: Thermal 3d gaussian splatting,” *arXiv preprint arXiv:2409.07200*, 2024.
- [8] Bernhard Kerbl, Georgios Kopanas, Thomas Leimkühler, and George Drettakis, “3d gaussian splatting for real-time radiance field rendering,” *ACM Trans. Graph.*, vol. 42, no. 4, pp. 139–1, 2023.
- [9] Zhifeng Gu and Bing Wang, “Mmone: Representing multiple modalities in one scene,” *arXiv preprint arXiv:2507.11129*, 2025.
- [10] Lukas Meyer, Josef Grün, Maximilian Weiherer, Bernhard Egger, Marc Stamminger, and Linus Franke, “Multi-spectral gaussian splatting with neural color representation,” *arXiv preprint arXiv:2506.03407*, 2025.
- [11] Zixiang Zhao, Haowen Bai, et al., “Cddfuse: Correlation-driven dual-branch feature decomposition for multi-modality image fusion,” in *Proceedings of the IEEE/CVF Conference on Computer Vision and Pattern Recognition*, June 2023, pp. 5906–5916.
- [12] Hui Li and Xiao-Jun Wu, “CrossFuse: A Novel Cross Attention Mechanism based Infrared and Visible Image Fusion Approach,” *Information Fusion*, vol. 103, pp. 102147, 2024.
- [13] Zixiang Zhao, Haowen Bai, Jiangshe Zhang, Yulun Zhang, Kai Zhang, Shuang Xu, Dongdong Chen, Radu Timofte, and Luc Van Gool, “Equivariant multi-modality image fusion,” in *Proceedings of the IEEE/CVF conference on computer vision and pattern recognition*, 2024, pp. 25912–25921.
- [14] Hui Li, Tianyang Xu, et al., “Lrrnet: A novel representation learning guided fusion network for infrared and visible images,” *IEEE transactions on pattern analysis and machine intelligence*, vol. 45, no. 9, pp. 11040–11052, 2023.
- [15] Yao Qian, Haojie Tang, Gang Liu, Mengliang Xing, Gang Xiao, and Durga Prasad Bavirisetti, “Limfusion: Infrared and visible image fusion via local information measurement,” *Optics and Lasers in Engineering*, vol. 181, pp. 108435, 2024.
- [16] Linfeng Tang, Jiteng Yuan, et al., “Piafusion: A progressive infrared and visible image fusion network based on illumination aware,” *Information Fusion*, vol. 83, pp. 79–92, 2022.
- [17] Naishan Zheng, Man Zhou, Jie Huang, Junming Hou, Haoying Li, Yuan Xu, and Feng Zhao, “Probing synergistic high-order interaction in infrared and visible image fusion,” in *Proceedings of the IEEE/CVF conference on computer vision and pattern recognition*, 2024, pp. 26384–26395.
- [18] Linfeng Tang, Jiteng Yuan, and Jiayi Ma, “Image fusion in the loop of high-level vision tasks: A semantic-aware real-time infrared and visible image fusion network,” *Information Fusion*, vol. 82, pp. 28–42, 2022.
- [19] Jiayi Ma, Linfeng Tang, Fan Fan, Jun Huang, Xiaoguang Mei, and Yong Ma, “Swinfusion: Cross-domain long-range learning for general image fusion via swin transformer,” *IEEE/CAA Journal of Automatica Sinica*, vol. 9, no. 7, pp. 1200–1217, 2022.